Acta Cryst. (1982). B**38**, 2555–2563

The Experimental Electron Density in Lithium Hydroxide Monohydrate*

BY KERSTI HERMANSSON AND JOHN O. THOMAS

Institute of Chemistry, University of Uppsala, Box 531, *S*-751 21 *Uppsala, Sweden*

(*Received* 28 *August* 1981; *accepted* 5 *May* 1982)

Abstract

The deformation electron density has been studied in $LiOH.H_2O$ at 295 K using a combination of X-ray and neutron diffraction data. Notoriously high extinction was present in the neutron data. Despite an attempt to reduce this by shock-cooling, the subsequent refinement of an extinction correction met with only partial success. Limited use was thus made of the neutron data in the determination of static multipole deformation density maps. The resulting peak maximum in the O—H bonds of the water molecule is 0·66 e $Å^{-3}$, and of the OH^- ion 0·49 e $Å^{-3}$. Lower peaks are observed in the lone-pair regions: 0·22 e $Å^{-3}$ for H_2O and 0·27 e $Å^{-3}$ for OH^-. These are to be compared with the results of theoretical *ab initio* calculations given by Hermansson & Lunell [*Acta Cryst.* (1982), B**38**, 2563–2569].

Introduction

This is the first of two papers dealing with the electron density in $LiOH.H_2O$. It describes an experimental study, and is followed in part II by a theoretical study (Hermansson & Lunell, 1982). The two sets of results are compared in part II.

The structure of $LiOH.H_2O$ was determined by Pepinsky (1939) and improved by Rabaud & Gay (1957) and Alcock (1971); all were film-data studies. The correct positions of the water H atoms were ascertained in a neutron diffraction study by Agron, Busing & Levy (1972).

We have collected X-ray and neutron diffraction data on $LiOH.H_2O$ at 295 K for the purpose of studying the deformation electron density in this compound. The tightly bound character of the structure makes it an appropriate candidate for an electron density study even at room temperature (see later). Since our neutron data were severely affected by extinction [this was not unexpected after the earlier work of Busing (1975)], we have attempted to reduce the extinction level in the crystals by repeated shock-cooling with liquid nitrogen. A second neutron data set (on a different crystal) has been collected. These two data sets, *without* and *with* shock-cooling, will be referred to as Neutron 1 and Neutron 2 in the following.

In view of the vital importance of a correct treatment of extinction in electron density studies, a comparison will be made between the distances and thermal parameters obtained from the different data sets (X-ray, Neutron 1 and Neutron 2 and Busing's neutron data) and using different refinement procedures. The deformation electron density maps will be discussed in the last section of this paper. These will be compared with theoretical *ab initio* deformation maps in part II. Preliminary results from this work were presented by Hermansson & Thomas (1979).

Crystal data

The crystals are monoclinic, space group $C2/m$, with cell dimensions $a = 7·4153$ (2), $b = 8·3054$ (2), $c = 3·1950$ (1) Å, $\beta = 110·107$ (4)°, $V = 184·78$ $Å^3$, $Z = 4$ (Agron, Busing & Levy, 1972).

Neutron data

Experimental and data reduction

Crystals were grown by very slow evaporation from a saturated aqueous solution of commercial $LiOH.H_2O$ *p.a.* Special care was taken to avoid contamination from CO_2 (aq.). The crystals used in the data collections were sealed in quartz-glass bulbs. The data collections were carried out on a Hilger & Watts four-circle diffractometer at the *R*2 Reactor at Studsvik, Sweden, where a double-monochromator [Cu, (220) plane] system gives a fixed wavelength of 1·210 Å. For a more detailed account of the experimental set-up see, for example, Hermansson, Thomas & Olovsson (1980). Some experimental details of the data collections are summarized in Table 1. For Neutron 1, an ω–2θ step-scanning procedure was used with a total scan interval in ω of 2·50° (determined empirically) for $\sin\theta/\lambda < 0·53$ $Å^{-1}$, and 3·00° for $0·53 < \sin\theta/\lambda < 0·69$ $Å^{-1}$. The corresponding scan widths for Neutron 2 were 2·00 and 2·25°, respectively. Three test reflections were used in both experiments. No

* Hydrogen Bond Studies. CXLIV.

0567-7408/82/102555-09$01.00

Table 1. *Experimental data and refinements*

	Neutron 1	Neutron 2	X-ray
Temperature (K)	295 (1)	295 (1)	295 (1)
Crystal volume (mm^3)	14·4	28·7	$2{\cdot}95 \times 10^{-3}$
μ (mm^{-1})	$\mu_{obs} = 0{\cdot}33$ (2)		$\mu_{calc} = 0{\cdot}085$
Transmission range	0·39–0·67	0·36–0·56	0·987–0·993
$\bar{T}_\mu$ range (mm)	1·09–2·24	1·59–2·86	0·09–0·15
λ (Å)	1·210		0·71069
$(\sin\theta/\lambda)_{max}$ ($Å^{-1}$)	0·69		1·05
Reflections measured	$\pm h \pm k\, l$	$h\, k \pm l$	$h \pm k \pm l$
No. of reflections measured	602	277	2125
No. of reflections with $\lvert F_o\rvert^2 > 2\sigma(\lvert F_o\rvert^2)$	518	227	720
No. of unique reflections measured	277	277	947
No. of parameters refined	38	38	(*A*) Conventional refinement 25
			(*B*) High-order refinement ($\sin\theta/\lambda > 0{\cdot}75$ $Å^{-1}$) 18
			(*C*) Deformation refinement 64
R^*_{w,F^2} (%), all reflections	7·6	6·7	(*A*) 6·6, (*B*) 6·6, (*C*) 3·7
$F_o^2 > 2\sigma(\lvert F_o\rvert^2)$	7·5	6·6	(*A*) 6·3, (*B*) 5·5, (*C*)3·2
S†	1·34	1·14	(*A*) 1·57, (*B*) 0·93, (*C*) 0·91

* $R_{w,F^2} = [\sum w(\lvert F_o\rvert^2 - \lvert F_c\rvert^2)^2 / \sum w(\lvert F_o\rvert^2)^2]^{1/2}$.
† $S = [\sum w(\lvert F_o\rvert^2 - \lvert F_c\rvert^2)^2/(m-n)]^{1/2}$, where m is the total number of reflections and n is the number of parameters refined.

significant variation was found for Neutron 2, but there was a total intensity decrease of 8% for the three test reflections of the Neutron 1 data set; a scaling function was thus applied to Neutron 1. Corrections for background intensity [peak-profile analysis according to Lehmann & Larsen (1974)], Lorentz factor and absorption were carried out [the effective absorption coefficient was measured as described in Hermansson, Thomas & Olovsson (1980)]. The agreement index, $R = (\sum \lvert\lvert F_o\rvert^2 - \langle\lvert F_o\rvert^2\rangle\rvert / \sum \lvert F_o\rvert^2)^{1/2}$, between symmetry related reflections (*hkl* and $\bar{h}\bar{k}\bar{l}$) for Neutron 1 was 0·03. Symmetry-related reflections were not averaged.

Refinements

Atomic positions from the Becker & Coppens (1975) refinement of Busing's neutron data were used as starting values in the full-matrix least-squares refinement program *UPALS* (Lundgren, 1979*a*). The quantity minimized was $\sum w(\lvert F_o\rvert^2 - \lvert F_c\rvert^2)^2$, where $w^{-1} = \sigma^2_{count}(\lvert F_o\rvert^2) + k^2\lvert F_o\rvert^4$, and σ_{count} was based on Poisson counting statistics. The quantity k was fixed empirically to 0·04 for Neutron 1, and to 0·05 for Neutron 2, in such a way that $\langle w(\lvert F_o\rvert^2 - \lvert F_c\rvert^2)^2\rangle$ was roughly equal for different intensity groups. The scattering lengths used were $b_H = -3{\cdot}74$, $b_{Li} = -1{\cdot}94$ and $b_O = 5{\cdot}80$ fm (Koester & Steyerl, 1977). Several extinction models were tried (see below). The parameters refined in the last cycles of refinement for both Neutron 1 and Neutron 2 were one scale factor, anisotropic extinction parameters and positional and anisotropic thermal parameters for all atoms (38 parameters in all). The extinction model used here employed the Becker & Coppens (1974) anisotropic Lorentzian type I formalism with a Thornley & Nelmes (1974) type mosaic-spread distribution. All reflections

Table 2. *Atomic positions in fractional coordinates* ($\times 10^5$)

For each coordinate the first row refers to Neutron 1, the second to Neutron 2, the third to the conventional spherical-atom X-ray refinement and the fourth to the X-ray deformation refinement.

	x	*y*	*z*
Li	0	34790 (26)	½
		34822 (27)	
		34797 (13)	
		34781 (8)	
O(1)	28600 (10)	0	39592 (32)
	28605 (11)		39519 (28)
	28608 (6)		39422 (14)
	28610 (8)		39545 (33)
O(*W*)	0	20668 (8)	0
		20669 (9)	
		20697 (5)	
		20685 (4)	
H(1)	26534 (27)	0	67367 (64)
	26514 (29)		67383 (58)
	27720 (205)		63972 (468)
	*		*
H(*W*)	11126 (16)	13264 (13)	13891 (48)
	11130 (17)	13286 (13)	13912 (41)
	9821 (116)	13996 (76)	13406 (287)
	*	*	*

* Not refined in the deformation refinement.

except some ten for which $y < 0{\cdot}10$ (where $|F_o|^2_{\text{uncorr.}} = y|F_o|^2_{\text{ext.corr.}}$) were included in the refinements. No feature left in the difference maps after the last cycles of refinement corresponds to >2% of the maximum peak height for O in an F_o synthesis map. Resulting R_{w,F^2} and S values from the two data sets are listed in Table 1. Atomic positional parameters are listed in Table 2. The thermal parameters are discussed below.*

Extinction

Several extinction models were applied to both data sets and the results compared on the basis of R_{w,F^2} values, S values, δR plots and σ considerations. We tested the Zachariasen (1967) extinction formalism, the Becker & Coppens (1974) formalism with isotropic, anisotropic, type I, type II, Lorentzian and Gaussian mosaic-spread distributions, using the distribution anisotropy according to Thornley & Nelmes (1974).

The extinction in $LiOH.H_2O$ was found to be anisotropic of type I (a type II model did converge but gave a decidedly worse fit; a general model did not converge). A Lorentzian mosaic-spread model was clearly preferred to a Gaussian.

It is well known that the Zachariasen model contains inadequacies (Becker & Coppens, 1974). It would therefore be natural to use the more correct Becker & Coppens model. We found that the *thermal parameters* were very dependent on the extinction model: the increases in the U_{ij} values of Neutron 1 were in the range 5–74% in going from an anisotropic Gaussian type I model in the Zachariasen formalism (Coppens & Hamilton, 1970) to an anisotropic Lorentzian type I model in the Becker & Coppens formalism (this difference was found to be due both to the differences between the Zachariasen and the Becker & Coppens models and to the differences between the Gaussian and the Lorentzian mosaic-spread models, but not to the errors in the Coppens & Hamilton treatment of mosaic anisotropy). This is illustrated by comparison of A and B in Fig. 1, which, for simplicity, displays only the equivalent isotropic r.m.s. amplitudes of vibration $\langle u^2\rangle^{1/2}$ (defined as the root of the arithmetic mean of the three principal values of the thermal vibrational tensor), resulting from refinements with different extinction models (the individual U_{ij} values behave in the same way). The same trend was observed by Becker & Coppens (1975) in their refinements of Busing's data.

Shock-cooling with liquid nitrogen prior to Neutron 2 proved successful in reducing the 'perfection' of our $LiOH.H_2O$ crystals and thereby also the extinction level. Table 3 shows the level of extinction in the two data sets. The reduction of the extinction level in Neutron 2 resulted in refined thermal parameters up to 40% larger than the Neutron 1 values (see B and D of Fig. 1). This is further discussed below.

We found that the refined nuclear *positions* were insensitive to the extinction model used.

Table 3. *Level of extinction (the percentage of reflections falling within various ranges of y, where y is given by* $|F_o|^2_{\text{uncorr.}} = y|F_o|^2_{\text{ext.corr.}}$)

Extinction model: Becker & Coppens formalism, anisotropic type I extinction with Thornley & Nelmes type Lorentzian mosaic-spread distribution.

	Neutron 1 (no shock cooling)	Neutron 2 (with shock cooling)
$0{\cdot}07 \le y \le 0{\cdot}25$	16%	4%
$0{\cdot}25 < y \le 0{\cdot}50$	36	20
$0{\cdot}50 < y \le 0{\cdot}75$	20	30
$0{\cdot}75 < y$	28	46

* Lists of temperature factors and structure factors for the Neutron 1, Neutron 2 and X-ray data sets have been deposited with the British Library Lending Division as Supplementary Publication No. SUP 36884 (24 pp.). Copies may be obtained through The Executive Secretary, International Union of Crystallography, 5 Abbey Square, Chester CH1 2HU, England.

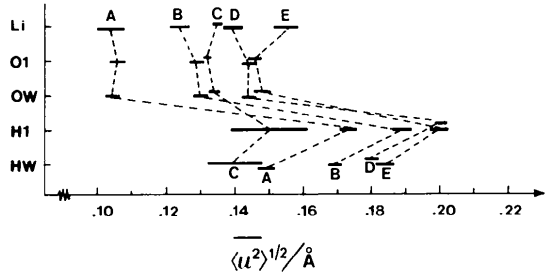

Fig. 1. Equivalent isotropic r.m.s. amplitudes of vibration for different data sets and different refinements for $LiOH.H_2O$. Error bars indicate $\pm 1\sigma$. (*A*) Neutron 1, Zachariasen anisotropic type I extinction model (Gaussian, Coppens & Hamilton type mosaic anisotropy). (*B*) Neutron 1, Becker & Coppens anisotropic type I extinction model (Lorentzian, Thornley & Nelmes type mosaic anisotropy). (*C*) X-ray, conventional refinement. (*D*) Neutron 2, Becker & Coppens anisotropic type I extinction model (Lorentzian, Thornley & Nelmes type mosaic anisotropy). (*E*) Busing & Levy's neutron data, Becker & Coppens anisotropic type I extinction model (Lorentzian, Thornley & Nelmes type mosaic anisotropy).

X-ray data

Experimental and data reduction

A small polyhedral crystal was mounted in a glass capillary. Intensity data were collected on a Stoe–Philips four-circle diffractometer using graphite-monochromatized Mo $K\alpha$ radiation. An ω–2θ step-scanning mode was used with a scan interval of $1{\cdot}0°$ in ω for all reflections. The time used for peak scanning varied between 75 and 300 s for different reflections, and the background was measured for 60 s at both limits of the scan interval. The intensity of the three test reflections

decreased linearly with time during the data collection, giving total intensity decreases of 3·5, 5·0 and 5·2%, respectively. One scaling function was applied to the whole data set.

The raw intensities were corrected for background, Lorentz, polarization and absorption effects. Symmetry-equivalent reflections were averaged. The agreement index between symmetry-related reflections, R, was 0·014.

Refinements

Different types of refinement of the X-ray data were carried out: (*A*) conventional spherical-atom refinements; (*B*) high-order refinements; (*C*) multipole deformation refinements.

The spherical-atom scattering factors used for H, Li^+ and O and the anomalous-dispersion correction for O were taken from *International Tables for X-ray Crystallography* (1974). Only eight reflections were weakened by more than 5% due to extinction; an isotropic type I extinction correction with Gaussian mosaic-spread distribution was applied (Gaussian and Lorentzian distributions gave equally good fits). The reflections were assigned weights in the refinement according to the formula $w^{-1} = \sigma^2_{\text{count}}(|F_o|^2) + k^2|F_o|^4$; k was fixed empirically at 0·02. The number of parameters refined and the resulting R_{w,F^2} values and S values are indicated for the different refinements in Table 1.

The three different types of refinement are discussed below.

(*A*) *Conventional refinement.* The parameters refined in the last cycle of refinement were one scale factor, one isotropic extinction parameter, positional parameters for all atoms and anisotropic (for non-hydrogen atoms) and isotropic (for H atoms) thermal parameters. The resulting atomic positional parameters are listed in Table 2. The average r.m.s. amplitudes of vibration are denoted by C in Fig. 1. Non-hydrogen positions agree with the neutron-diffraction-determined positions except for the small asphericity shifts of 0·006 (1) and 0·003 (1) Å which occur towards the lone-pair regions for O(1) and O(W), respectively.

(*B*) *High-order refinements.* High-order refinement using the 766 reflections with $\sin\theta/\lambda > 0{\cdot}60$ Å^{-1} or the 595 reflections with $\sin\theta/\lambda > 0{\cdot}75$ Å^{-1} gave the same positional and thermal non-hydrogen parameters as the conventional refinement, except that the O(1) and O(W) atoms have moved closer to the neutron-determined positions compared to the results from the conventional X-ray refinement. The asphericity shifts for O(1) and O(W) are now 0·003 (1) and 0·001 (1) Å, respectively. For the 0·75 Å^{-1} cut-off, it was not meaningful to refine the H parameters; these were kept fixed at their Neutron 1 values. For the 0·60 Å^{-1} cut-off, the resulting O(1)–H(1) and O(W)–H(W) distances were 0·82 (3) and 0·82 (2) Å, respectively, as compared to 0·830 (10) and 0·895 (5) Å from the conventional refinement; *i.e.* the high-order refinement did not result in more correct H positions.

(*C*) *Deformation refinements.* The deformation refinement used parameterizes the redistribution of electron density in the crystal with respect to a reference state of superimposed free ground-state spherical atoms (or ions). The calculated static total electron distribution, $\rho_c^{\text{stat}}(\mathbf{r})$, is written as a sum of the non-vibrating spherical-atom (ion) densities and the electron density deformation which is expanded into a set of multipolar functions, $\delta\rho_{ij}^{\text{stat}}(\mathbf{r})$, centred on each atom (or ion) i, such that:

$$\rho_c^{\text{stat}}(\mathbf{r}) = \sum_{\text{atom } i} \rho_{i,\text{sph}}^{\text{stat}}(\mathbf{r}) + \sum_{\text{atom } i} \sum_{\text{def.fn. } j} c_{ij}\,\delta\rho_{ij}^{\text{stat}}(\mathbf{r}). \quad (1)$$

The dynamical density is obtained if, for each atom i, the appropriate atomic vibrational tensor is applied to the spherical-atom density and the multipole deformation functions centred on atom i.

The Fourier transforms of the multipolar functions are added to the normal spherical-atom scattering factors in the least-squares refinement including variation of the coefficient c_{ij}. The expression $\sum\sum c_{ij}\,\delta\rho_{ij}^{\text{stat}}(\mathbf{r})$ is plotted in the static electron deformation model maps.

We have used the deformation functions of Hirshfeld (1971), where the deformation functions corresponding to static atoms have the form:

$$\delta\rho_{ij}^{\text{stat}}(r,\theta,n,k) = \begin{cases} N_n\, r^n\, e^{-\gamma r^2} \cos^n\theta_k & \text{(Gaussian radial function)} \\ \text{or} & \\ N_n\, r^n\, e^{-\alpha r} \cos^n\theta_k & \text{(exponential radial function).} \end{cases}$$

Here, N_n is a normalization factor, r is the distance from the atom centre, n is an integer ≥ 0, and θ_k is the angle between $\mathbf{r}$ and the polar axis $\mathbf{k}$ [which is one of a set of $(n+1)(n+2)/2$ polar axes distributed in space].

Deformation refinements using exponential functions were found to show poor convergence, so that Gaussian radial functions were used exclusively.

The exponents (γ) and coefficients of terms in (1) up to the octapole level ($n \leq 3$) were refined for Li^+, O(1) and O(W), and for H(1) and H(W) up to the quadrupole level ($n \leq 2$). The octapolar coefficients for Li^+ were all less than 1σ. The refined Gaussian exponents were 1·0 (1), 4·4 (3), 4·0 (5), 4·3 (5) and 5·9 (10) Å^{-2} for Li^+, O(1), O(W), H(1) and H(W), respectively.

Crystallographic site-symmetry restrictions only were applied to the deformation functions centred on the Li^+, O(1) and O(W) atoms. Axial symmetry about the OH bonds was assumed for H(1) and H(W).

The postional and thermal parameters were refined for the non-hydrogen atoms, along with the defor-

mation coefficients. For the H atoms, the positional and thermal parameters were fixed at their refined neutron values. The resulting deformation densities were found to be almost identical irrespective of whether we took the H parameters from Neutron 1 or Neutron 2.

The inclusion of deformation functions represents a significant improvement to the conventional spherical-atom model. This is seen from the R_{w,F^2} values, S values, δR plots and the residual maps. The scale factors (on F_o) resulting from the deformation refinement and the conventional refinement differed by less than 1%. In the residual maps [including only reflections with $|F_o|^2 > 3\sigma(|F_o|^2)$] after the conventional refinements, the quantity $|\rho_o(\mathbf{r}) - \rho_c(\mathbf{r})|$ was $<0{\cdot}20$ e Å^{-3}, and for the deformation refinement $|\rho_o(\mathbf{r}) - \rho_c(\mathbf{r})|$ was $<0{\cdot}07$ e Å^{-3}. The residual map is surprisingly flat for the conventional refinement. This must be due to the very small, yet quite evidently important, positional and thermal parameter shifts which occur in the conventional refinement to compensate for bonding and lone-pair density effects (see Lundgren, 1979*b*). In the spherical-atom refinement, six reflections had $||F_o|^2 - |F_c|^2|/\sigma(|F_o|^2)$ values between 5·0 and 10·0 and one reflection had a value of 25·0. After the deformation refinement none of these values was larger than 4·0.

Non-hydrogen positions resulting from the deformation refinement agree to within 1σ with those from the high-order X-ray refinement. The non-hydrogen thermal parameters from all three types of X-ray refinement agree to within 3σ; these differ significantly from the neutron thermal parameters, however (see Fig. 1).

We wanted to examine whether the discrepancy between thermal parameters from the neutron refinements and from the X-ray deformation refinement was in part a result of too inflexible a deformation model. We therefore included a type of 'core deformation' by introducing onto each atom a second monopolar and dipolar function with the Gaussian radial exponent arbitrarily set to 15·0 Å^{-2} [*cf.* the core polarization treatment of parabanic acid by Craven & McMullan (1979)]. The correlations obtained were very large and the refined U_{ij} values agreed with those obtained with the old deformation model. The introduction of higher-order (hexadecapolar) functions was tested on O(W) in order to investigate their effect on the thermal parameters; all the resulting hexadecapolar coefficients were smaller than their estimated standard deviations and the thermal parameters were unaffected by this procedure.

Comparison of results from the different data sets

A stereoscopic picture of the crystal structure is presented in Fig. 2. The resulting atomic positions

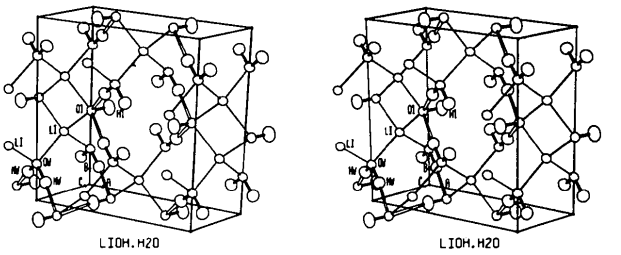

Fig. 2. A stereoscopic picture of the structure of $LiOH.H_2O$ (as derived from the Neutron 1 refinement). The thermal ellipsoids are drawn to include 50% probability. Covalent bonds are filled, H···O bonds are open and ionic bonds are drawn as single lines.

agree within 2σ for the three neutron data sets considered: Neutron 1, Neutron 2 and Busing's data (Becker & Coppens, 1975). Apart from the expected large disagreement between the H positions [0·161 (14) Å for H(1) and 0·111 (8) Å for H(W)], there are no large discrepancies between the positions resulting from the X-ray refinements and the neutron data. The conventional X-ray refinement yields an O(1) atomic position which is shifted 0·006 (1) Å towards the lone-pair region as compared to the neutron-determined position, but the asphericity shifts are less than 0·003 (1) Å for the high-order and deformation refinements.

Thermal parameters disagree significantly between the four data sets. This is illustrated by B, C, D and E in Fig. 1. The thermal parameters from Neutron 2 are higher than those from Neutron 1 as a result of the decrease in the level of extinction. The ratios between the mean-square vibrational amplitudes U_{ij}(Neutron 2)/U_{ij}(Neutron 1) lie in the range 1·01–1·44. The agreement between Busing's data and Neutron 2 is somewhat better: the U_{ij}(Busing) ratios lie in the range 0·82–1·09. Neither Neutron 1 nor Neutron 2 (nor Busing's data) agree with the X-ray results: the U_{ij} values from Neutron 1 are up to 20% lower than the X-ray values, and the Neutron 2 values are up to 20% above the X-ray values.

On the whole, Fig. 1 paints a rather dismal picture. Large discrepancies of this type between X-ray and neutron thermal parameters have been found in many other studies. Reasons commonly cited for these differences are a temperature mismatch, different TDS contributions, and different extinction effects. Extinction can be expected to be the most likely explanation in the present case. Because of the large differences between X-ray and neutron thermal parameters and the different results from different neutron data sets, we have tried to rely as little as possible on neutron parameters for our charge deformation maps. A series of X–N maps were, in fact, calculated and readily seen to be seriously affected by the systematic errors in scale factors and temperature parameters. Our discussion will, therefore, be based on the maps resulting from the multipole deformation refinement

where neutron parameters (positional and thermal) have been used only for the H atoms.

Deformation maps

Static multipole deformation maps are presented in Figs. 3, 4(*a*) and 5. These model maps have been calculated using the double Fourier procedure, *i.e.* the maps are F_c synthesis maps where the F_c's include only the contributions from the deformation functions. Only F_c values for the measured reflections (*i.e.* $\sin\theta/\lambda \leq 1{\cdot}05$ Å^{-1}) were included in the summation. Syntheses calculated for $\sin\theta/\lambda \leq 0{\cdot}90$ Å^{-1} were almost identical, implying a negligible influence from the data above $\sin\theta/\lambda = 0{\cdot}90$ Å^{-1}.

The *static* deformation maps are obtained by setting the temperature factors equal to zero in the F_c synthesis. This way of deconvoluting the experimental dynamical electron density to separate out asphericity caused by thermal vibrations and static defomation is by no means ideal. In addition to the fundamental question of the validity of the convolution approximation (see, for example, Hirshfeld, 1977) there is the more technical problem of strong correlation between thermal parameters, deformation parameters and scale

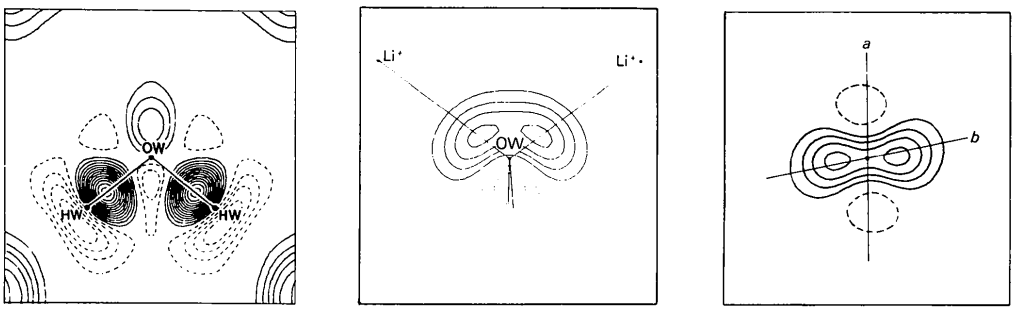

(*a*) (*b*) (*c*)

Fig. 3. Static multipole model maps for the H_2O molecule in $LiOH.H_2O$. The contour interval is 0·05 e Å^{-3}. Negative contours are dashed and the zero contour is omitted. The subtracted reference atoms or ions are Li^+, O and H in all maps. (*a*) Section through the H_2O molecular plane. (*b*) Section through the Li^+—O(*W*)—Li^+ plane. (*c*) Section through a plane normal to the bisector of the H(*W*)—O(*W*)—H(*W*) angle and passing 0·25 Å above the O(*W*) atom. The line *a* indicates the positions of the projections of the H(*W*) atoms onto the plane. The line *b* indicates the positions of the projections of the Li^+ ions onto the plane.

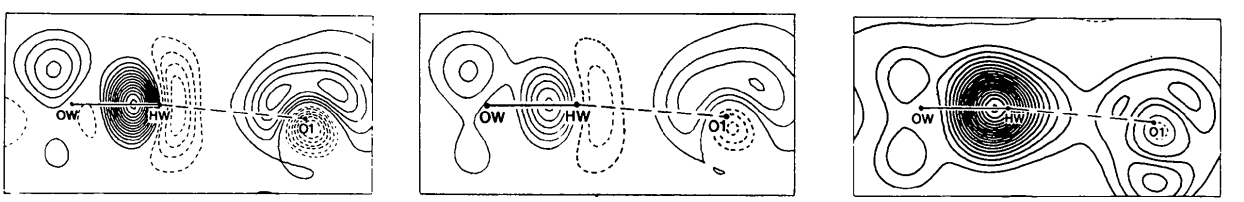

(*a*) (*b*) (*c*)

Fig. 4. (*a*) Static multipole model map through the hydrogen bond [O(*W*)—H(*W*)···O(1)]. (*b*) Dynamic multipole model map through the hydrogen bond [O(*W*)—H(*W*)···O(1)]. (*c*) Same as (*b*), except the H-atom electron density is not subtracted. Contour levels are as in Fig. 3.

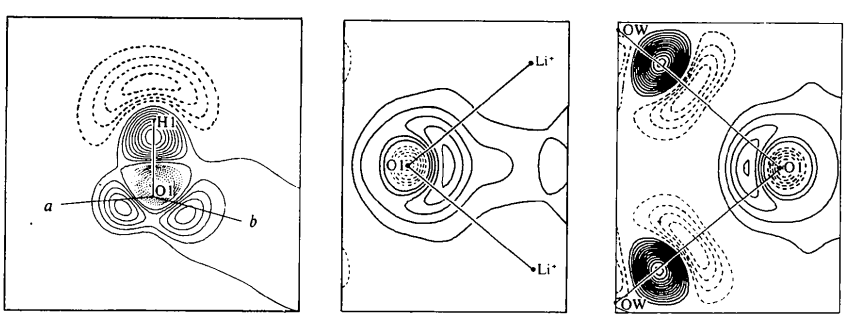

(*a*) (*b*) (*c*)

Fig. 5. Static multipole model maps for the OH^- ion in $LiOH.H_2O$. Contour levels are as in Fig. 3. (*a*) In the mirror plane containing OH^- [line *a* indicates the intersection with a plane containing the two O(*W*) neighbours and line *b* the intersection with a plane containing the two Li^+ neighbours]. (*b*) In the Li^+—O(1)—Li^+ plane. (*c*) In the O(*W*)···O(1)···O(*W*) plane.

factor; this affects the reliability of the individual parameters refined. Neither are the *dynamic* multipole deformation maps unaffected by this correlation: the reference state of superimposed thermally smeared spherical atoms is directly dependent on the thermal parameters (chosen or refined). We have chosen to present static deformation maps in this paper, largely because we will be comparing them with theoretically calculated static maps in the following paper.

In this connection it is relevant to consider the magnitude of the thermal motion of the atoms in the compound studied, since it is an advantage to have a low level of thermal motion. In $LiOH.H_2O$ at 295 K the equivalent isotropic r.m.s. amplitudes of vibration (X-ray values for non-hydrogen atoms and average values between Neutron 1 and Neutron 2 for H atoms) are 0·135, 0·132, 0·134, 0·194 and 0·174 Å for Li, O(1), O(*W*), H(1) and H(*W*), respectively. These values can be compared with the thermal vibrational amplitudes in α-$(COOH)_2.2H_2O$ at 100 K (Stevens & Coppens, 1980), where the average r.m.s. amplitudes of vibration (derived from high-order X-ray data) are 0·099, 0·116, 0·116 and 0·115 Å for C(1), O(1), O(2) and O(3), respectively, and 0·168, 0·185 and 0·191 Å, respectively, for the three H atoms (neutron values multiplied by the average ratio of the X-ray-determined to neutron-diffraction-determined thermal parameters for the C and O atoms). As far as thermal motion is concerned, it can thus be argued that the tighter-bound character of $LiOH.H_2O$ makes it almost as suitable a candidate for electron density studies at room temperature as α-$(COOH)_2.2H_2O$ is at 100 K.

In the deformation maps presented below, the reference state consists of the neutral spherically averaged O and H atoms and the Li^+ ion. The integrated deformation density around the OH^- ion should thus contain an excess charge of one electron. No explicit estimate has been made of the errors in the present deformation density maps.

Discussion

Agron, Busing & Levy (1972) describe the structure of $LiOH.H_2O$ as consisting of pairs of Li^+ ions joined by two bridging OH^- ions to form rhombic units approximately parallel to the *ab* plane. These units are linked in the **c** direction by the water molecules.

The H_2O *molecule*

The water O atom lies on a twofold rotation axis. The water molecule is approximately tetrahedrally surrounded by two Li^+ ions and two OH^- ions (see Fig. 2; distances are listed in Table 4). The *static* multipole deformation density for H_2O is displayed in Fig. 3(*a*)–(*c*). There is excess density in the OH bonds and in the lone-pair region with maximum peak heights 0·66 and 0·22 e Å^{-3}, respectively. The corresponding *dynamical* multipole maps look very similar except that all peaks are lower and all troughs shallower. The maximum dynamical deformation density in the water OH peaks is 0·31 e Å^{-3} and in the O lone-pair region 0·17 e Å^{-3}. The Li^+—O(*W*)—Li^+ plane makes an angle of 11·7° with the plane bisecting the water angle. Fig. 3(*c*) shows that the lone-pair deformation density does not have its maxima *in* the Li^+—O(*W*)—Li^+ plane, but rather closer to a plane perpendicular to the H_2O molecule. This feature will be further discussed in part II.

Table 4. *Distances* (Å) *and angles* (°) *from the Neutron* 1 *refinements*

The indices (*a*)–(*f*) imply the following symmetry operations: (*a*) $x+\frac{1}{2}, \frac{1}{2}-y, z$; (*b*) $x, y, z-1$; (*c*) $x+\frac{1}{2}, y-\frac{1}{2}, z$; (*d*) $x, y, z+1$; (*e*) $\bar{x}, y, \bar{z}$; (*f*) $x, \bar{y}, z$.

O(*W*)–H(*W*)	1·002 (1)	H(*W*)–O(*W*)–H(*W*)^e	104·3 (1)
O(*W*)···O(1)	2·683 (1)	O(1)–O(*W*)–O(1)^e	100·5 (1)
H(*W*)···O(1)	1·684 (1)	Li–O(*W*)–Li^b	107·4 (1)
O(*W*)–Li	1·982 (1)	Li–O(*W*)–H(*W*)	103·6 (1)
O(1)–H(1)	0·951 (2)	Li–O(*W*)–H(*W*)^e	119·5 (1)
O(1)–Li^a	1·965 (1)	O(*W*)–H(*W*)···O(1)	174·8 (1)
O(1)···O(1)^d	3·1950 (1)	Li^a–O(1)–Li^c	80·0 (1)
H(1)···O(1)^d	2·259 (2)	Li^a–O(1)–H(*W*)	95·9 (1)
		H(*W*)···O(1)···H(*W*)^f	81·7 (1)
		Li^a–O(1)–H(1)	102·8 (1)
		H(1)–O(1)···H(*W*)	96·4 (1)
		O(1)–H(1)···O(1)^d	167·6 (2)

The lone-pair region of O(*W*) consists of two barely resolved maxima at 0·45 Å from the nucleus. Both for an isolated H_2O molecule and for the H_2O molecule in $LiOH.H_2O$ the theoretical calculations (see part II) show that the deformation density in the O(*W*) lone-pair region consists of two pronounced peaks very close to the O nuclei, but show no tendency for double-peaking further out in the region corresponding to the two maxima in Fig. 3(*b*). Other experimental deformation density studies on hydrates have given examples of both single and double maxima in the water O lone-pair regions.

Stevens & Coppens (1980) and Hermansson & Lunell (1981) have listed references to previous experimental deformation density studies of crystalline hydrates. The density features for the water molecules show substantial variations; much larger than might reasonably be expected to result from the different surroundings (see part II).

In the present study, the O(*W*) lone-pair deformation density would appear to be too low. This judgement is based on a comparison both with the experimental O(*W*)—H(*W*) bond deformation density and with the theoretical lone-pair density of a free H_2O molecule.

Although theoretical calculations show that the environment causes a *decrease* in the O lone-pair density for H_2O in $LiOH.H_2O$ as compared to a free

H_2O molecule [see Hermansson & Lunell (1981), and part II], they do not altogether explain the low experimental deformation density found in this region.

The deformation density features in the O lone-pair region are inherently rather uncertain. Combined with the difficulty of making experimental (diffraction) observations of features close to the nuclei, there is the related problem of large correlations in the multipole refinement. Consider, for example, the experimentally observed *dynamic* density which will tend to lack sharp features as a result of thermal smearing and limitations in experimental resolution: correlation effects can then bring about an incomplete deconvolution of the *static* deformation and thermal motion. This can lead, in turn, to a smoothing of the static electron density features (*cf.* Rees, 1977).

The problems of correlation become particularly severe very close to the nuclei, where the deformation density can be partly accounted for by small shifts in the nuclear positions and thermal parameters. Reliable information about the deformation density in those regions (where, for example, the concentrated lone-pair maxima are situated in the theoretical deformation maps) is thus inaccessible with the present technique.

A further possible explanation for low lone-pair deformation density features is an inflexibility in the deformation functions to take proper account simultaneously of both lone-pair peaks and bond peaks. This was discussed by Stevens & Coppens (1980) in connection with their multipole model refinements on α-$(COOH)_2.2H_2O$.

That the experimental static deformation density in the O lone-pair regions is much lower than the OH bond peaks can also be explained partly (at least in principle) by the bond peaks, in fact, being too high. The deformation density in the OH bond region is described by multipole functions centred on both the O and the H atom. If the deformation functions centred on the H atom make an unduly large contribution to the description of the dynamic bond density as a consequence of large correlation in the multipole refinement, the resulting *static* bond deformation density will be too high, since the H multipole functions are deconvoluted (from the dynamic density) using much larger temperature factors than the O-atom functions.

The hydrogen bond

The hydrogen bond in $LiOH.H_2O$ is rather strong [$O(W)\cdots O(1)$ 2·683 Å, $O(W)$–$H(W)\cdots O(1)$ 174·8°]. The static multipole deformation density in the plane through the hydrogen bond is shown in Fig. 4(*a*). The dynamical maps in Figs. 4(*b*) and 4(*c*) are included to facilitate a comparison with published experimental X–N or X–$X_{\text{high-order}}$ maps for other compounds. The spherical H atom has *not* been subtracted in Fig. 4(*c*). Such maps have been published for a few hydrogen-bonded compounds and suggest that, for short hydrogen bonds, there is a continuous ridge of electron density in the $H\cdots O$ region, while for longer hydrogen bonds this density is close to zero. Figs. 4(*a*) and 4(*b*) display features typical of weak or intermediate hydrogen bonds: electron excess in the O–H bond and in the lone-pair region of the hydrogen-bond acceptor and an electron deficiency on the weakly bonded side of the H atom.

The OH^- *ion*

The OH^- ion lies in a mirror plane. The O atom is bonded to two Li^+ ions [O(1)–Li^+ 1·965 Å] and through hydrogen bonds to two H_2O molecules. There is a weaker hydrogen bond [$O(1)\cdots O(1)$ 3·195 Å, $O(1)$–$H(1)\cdots O(1)$ 167·6°] joining OH^- ions in neighbouring unit cells. The deformation density maps for OH^- in the mirror plane, in the Li^+–O(1)–Li^+ plane, and in the $O(W)\cdots O(1)\cdots O(W)$ plane are displayed in Figs. 5(*a*)–(*c*), respectively.

There is excess deformation density in the OH bond and in the lone-pair region (maximum peak heights: 0·49 and 0·27 e $Å^{-3}$, respectively), and a deficiency on the weakly bonded side of the H atom.

Mair (1978) has studied the dynamic electron density distribution in LiOH. The O atom in LiOH is surrounded by four Li^+ ions at a distance of 1·963 Å, *i.e.* the environment of the OH^- ion resembles that in $LiOH.H_2O$. It should be noted that the reference state for O used in Mair's maps is O^- as compared to O in our maps. This places no serious limitation on a comparison between the two studies, however, since the difference between the Hartree–Fock electron densities of O and O^- is not greater than ~0·10 e $Å^{-3}$ at a distance greater than 0·10 Å from the oxygen nuclei.

There are significant discrepancies, however, between Mair's results and ours; especially on the weakly bonded side of the OH^- H atom (Fig. 2 of Mair's paper), where an electron excess of ~0·13 e $Å^{-3}$ is found, in contrast to an electron deficiency of −0·17 e $Å^{-3}$ in our dynamic density distribution (*cf.* our Fig. 5*a*, which displays the static deformation density).

A more thorough discussion of the chemical implications of our results, particularly in relation to the effect of intramolecular bonding on the electron density, is given in part II, where we draw heavily on supporting results obtained from theoretical calculations.

We wish to thank Professor Ivar Olovsson for his interest in this work and for the facilities placed at our disposal. We are also indebted to Dr Roland Tellgren for valuable help with the neutron data collections and to Mr Hilding Karlsson for skilled technical assistance. Drs Jörgen Tegenfeldt and Torbjörn Gustafsson are gratefully acknowledged for many stimulating discussions, as is Dr Garry McIntyre.

Financial support provided by the Swedish Natural Science Research Council and the Lennander foundation is gratefully acknowledged.

References

AGRON, P. A., BUSING, W. R. & LEVY, H. A. (1972). Abstracts. Winter Meet. Am. Crystallogr. Assoc., Albuquerque, New Mexico, p.52.

ALCOCK, N. W. (1971). *Acta Cryst.* B**27**, 1682–1683.

BECKER, P. & COPPENS, P. (1974). *Acta Cryst.* A**30**, 129–147.

BECKER, P. & COPPENS, P. (1975). *Acta Cryst.* A**31**, 417–425.

BUSING, W. R. (1975). Private communication.

COPPENS, P. & HAMILTON, W. C. (1970). *Acta Cryst.* A**26**, 71–83.

CRAVEN, B. M. & MCMULLAN, R. K. (1979) *Acta Cryst.* B**35**, 934–945.

HERMANSSON, K. & LUNELL, S. (1981). *Chem. Phys. Lett.* **80**, 64–68.

HERMANSSON, K. & LUNELL, S. (1982). *Acta Cryst.* B**38**, 2563–2569.

HERMANSSON, K. & THOMAS, J. O. (1979). Abstracts. Fifth Eur. Crystallogr. Meet., Copenhagen, Denmark, p. 351.

HERMANSSON, K., THOMAS, J. O. & OLOVSSON, I. (1980). *Acta Cryst.* B**36**, 1032–1040.

HIRSHFELD, F. L. (1971). *Acta Cryst.* B**27**, 769–781.

HIRSHFELD, F. L. (1977). *Isr. J. Chem.* **16**, 168–174.

International Tables for X-ray Crystallography (1974). Vol. IV, pp. 72–73, 149. Birmingham: Kynoch Press.

KOESTER, L. & STEYERL, A. (1977). *Neutron Physics*, p. 36. Berlin, Heidelberg, New York: Springer.

LEHMANN, M. S. & LARSEN, F. K. (1974). *Acta Cryst.* A**30**, 580–584.

LUNDGREN, J.-O. (1979*a*). *Crystallographic Computer Programs*. Report UUIC-B13-04-04, Institute of Chemistry, Univ. of Uppsala.

LUNDGREN, J.-O. (1979*b*). *Acta Cryst.* B**35**, 1027–1033.

MAIR, S. L. (1978). *Acta Cryst.* A**34**, 542–547.

PEPINSKY, R. (1939). *Z. Kristallogr.* **102**, 119–131.

RABAUD, H. & GAY, R. (1957). *Bull. Soc. Fr. Minéral. Cristallogr.* **80**, 166–180.

REES, B. (1977). *Isr. J. Chem.* **16**, 180–186.

STEVENS, E. D. & COPPENS, P. (1980). *Acta Cryst.* B**36**, 1864–1876.

THORNLEY, F. R. & NELMES, R. J. (1974). *Acta Cryst.* A**30**, 748–757.

ZACHARIASEN, W. H. (1967). *Acta Cryst.* **23**, 558–564.

Acta Cryst. (1982). B**38**, 2563–2569

The Theoretical Electron Density in Lithium Hydroxide Monohydrate*

BY KERSTI HERMANSSON

Institute of Chemistry, University of Uppsala, Box 531, *S*-751 21 *Uppsala, Sweden*

AND STEN LUNELL

Department of Quantum Chemistry, University of Uppsala, Box 518, *S*-751 20 *Uppsala, Sweden*

(*Received* 28 *August* 1981; *accepted* 3 *March* 1982)

Abstract

The electron density in $LiOH.H_2O$ has been determined by *ab initio* MO–LCAO–SCF calculations. All nearest neighbours to the H_2O molecule and the OH^- ion, respectively, have been included explicitly in the calculations; next-nearest and more-distant neighbours have been simulated by point charges. The theoretical electron density maps are compared with experimental maps [Hermansson & Thomas (1982). *Acta Cryst.* B**38**, 2555–2563] with good overall agreement. The influence of intermolecular bonding in the crystal is found to be twofold. Firstly, the overall polarization of the H_2O molecule and the OH^- ion is increased significantly. Secondly, the electron density around the O nuclei in H_2O and OH^- is rearranged, leading to a decrease of density in the lone-pair directions. The reasons for this decrease are discussed in some detail.

Introduction

This paper is part II of an experimental and theoretical study of the electron density in $LiOH.H_2O$.

In part I (Hermansson & Thomas, 1982), the redistribution of electrons occurring on bond formation in $LiOH.H_2O$ was discussed in terms of deformation density maps. These displayed the deviation of the total experimental electron density from a calculated reference state of superposed spherically averaged

* Hydrogen Bond Studies. CXLV.

0567-7408/82/102563-07$01.00